Measurement of the quasi-elastic axial vector mass in neutrino interactions on oxygen

R. Gran,[33, *] E. J. Jeon,[24] E. Aliu,[1] S. Andringa,[1] S. Aoki,[14] J. Argyriades,[5] K. Asakura,[14] R. Ashie,[29]
F. Berghaus,[3] H. Berns,[33] H. Bhang,[24] A. Blondel,[9] S. Borghi,[9] J. Bouchez,[5] J. Burguet-Castell,[32] D. Casper,[4]
J. Catala,[32] C. Cavata,[5] A. Cervera,[9] S. M. Chen,[31] K. O. Cho,[6] J. H. Choi,[6] U. Dore,[23] X. Espinal,[1] M. Fechner,[5]
E. Fernandez,[1] Y. Fukuda,[19] J. Gomez-Cadenas,[32] T. Hara,[14] M. Hasegawa,[16] T. Hasegawa,[26] K. Hayashi,[16]
Y. Hayato,[29] R. L. Helmer,[31] K. Hiraide,[16] J. Hosaka,[29] A. K. Ichikawa,[11] M. Iinuma,[12] A. Ikeda,[21] T. Inagaki,[16]
T. Ishida,[11] K. Ishihara,[29] T. Ishii,[11] M. Ishitsuka,[30] Y. Itow,[29] T. Iwashita,[11] H. I. Jang,[6] I. S. Jeong,[6] K. K. Joo,[24]
G. Jover,[1] C. K. Jung,[27] T. Kajita,[30] J. Kameda,[29] K. Kaneyuki,[30] I. Kato,[31] E. Kearns,[2] D. Kerr,[27] C. O. Kim,[15]
M. Khabibullin,[13] A. Khotjantsev,[13] D. Kielczewska,[34, 25] J. Y. Kim,[6] S. B. Kim,[24] P. Kitching,[31] K. Kobayashi,[27]
T. Kobayashi,[11] A. Konaka,[31] Y. Koshio,[29] W. Kropp,[4] J. Kubota,[16] Yu. Kudenko,[13] Y. Kuno,[22] Y. Kurimoto,[16]
T. Kutter,[17, 3] J. Learned,[10] S. Likhoded,[2] I. T. Lim,[6] P. F. Loverre,[23] L. Ludovici,[23] H. Maesaka,[16] J. Mallet,[5]
C. Mariani,[23] S. Matsuno,[10] V. Matveev,[13] K. McConnel,[18] C. McGrew,[27] S. Mikheyev,[13] A. Minamino,[29]
S. Mine,[4] O. Mineev,[13] C. Mitsuda,[29] M. Miura,[29] Y. Moriguchi,[14] T. Morita,[16] S. Moriyama,[29] T. Nakadaira,[11]
M. Nakahata,[29] K. Nakamura,[11] I. Nakano,[21] T. Nakaya,[16] S. Nakayama,[30] T. Namba,[29] R. Nambu,[29] S. Nawang,[12]
K. Nishikawa,[16] K. Nitta,[11] F. Nova,[1] P. Novella,[32] Y. Obayashi,[29] A. Okada,[30] K. Okumura,[30] S. M. Oser,[3]
Y. Oyama,[11] M. Y. Pac,[7] F. Pierre,[5] A. Rodriguez,[1] C. Saji,[30] M. Sakuda,[21] F. Sanchez,[1] A. Sarrat,[27] T. Sasaki,[16]
H. Sato,[16] K. Scholberg,[8, 18] R. Schroeter,[9] M. Sekiguchi,[14] M. Shiozawa,[29] K. Shiraishi,[33] G. Sitjes,[32] M. Smy,[4]
H. Sobel,[4] M. Sorel,[32] J. Stone,[2] L. Sulak,[2] A. Suzuki,[14] Y. Suzuki,[29] T. Takahashi,[12] Y. Takenaga,[30] Y. Takeuchi,[29]
K. Taki,[29] Y. Takubo,[22] N. Tamura,[20] M. Tanaka,[11] R. Terri,[27] S. T'Jampens,[5] A. Tornero-Lopez,[32] Y. Totsuka,[11]
S. Ueda,[16] M. Vagins,[4] L. Whitehead,[27] C.W. Walter,[8] W. Wang,[2] R.J. Wilkes,[33] S. Yamada,[29] S. Yamamoto,[16]
C. Yanagisawa,[27] N. Yershov,[13] H. Yokoyama,[28] M. Yokoyama,[16] J. Yoo,[24] M. Yoshida,[22] and J. Zalipska[25]

(The K2K Collaboration)

[1]*Institut de Fisica d'Altes Energies, Universitat Autonoma de Barcelona, E-08193 Bellaterra (Barcelona), Spain*
[2]*Department of Physics, Boston University, Boston, Massachusetts 02215, USA*
[3]*Department of Physics & Astronomy, University of British Columbia, Vancouver, British Columbia V6T 1Z1, Canada*
[4]*Department of Physics and Astronomy, University of California, Irvine, Irvine, California 92697-4575, USA*
[5]*DAPNIA, CEA Saclay, 91191 Gif-sur-Yvette Cedex, France*
[6]*Department of Physics, Chonnam National University, Kwangju 500-757, Korea*
[7]*Department of Physics, Dongshin University, Naju 520-714, Korea*
[8]*Department of Physics, Duke University, Durham, North Carolina 27708, USA*
[9]*DPNC, Section de Physique, University of Geneva, CH1211, Geneva 4, Switzerland*
[10]*Department of Physics and Astronomy, University of Hawaii, Honolulu, Hawaii 96822, USA*
[11]*High Energy Accelerator Research Organization(KEK), Tsukuba, Ibaraki 305-0801, Japan*
[12]*Graduate School of Advanced Sciences of Matter, Hiroshima University, Higashi-Hiroshima, Hiroshima 739-8530, Japan*
[13]*Institute for Nuclear Research, Moscow 117312, Russia*
[14]*Kobe University, Kobe, Hyogo 657-8501, Japan*
[15]*Department of Physics, Korea University, Seoul 136-701, Korea*
[16]*Department of Physics, Kyoto University, Kyoto 606-8502, Japan*
[17]*Department of Physics and Astronomy, Louisiana State University, Baton Rouge, Louisiana 70803-4001, USA*
[18]*Department of Physics, Massachusetts Institute of Technology, Cambridge, Massachusetts 02139, USA*
[19]*Department of Physics, Miyagi University of Education, Sendai 980-0845, Japan*
[20]*Department of Physics, Niigata University, Niigata, Niigata 950-2181, Japan*
[21]*Department of Physics, Okayama University, Okayama, Okayama 700-8530, Japan*
[22]*Department of Physics, Osaka University, Toyonaka, Osaka 560-0043, Japan*
[23]*University of Rome La Sapienza and INFN, I-000185 Rome, Italy*
[24]*Department of Physics, Seoul National University, Seoul 151-747, Korea*
[25]*A. Soltan Institute for Nuclear Studies, 00-681 Warsaw, Poland*
[26]*Research Center for Neutrino Science, Tohoku University, Sendai, Miyagi 980-8578, Japan*
[27]*Department of Physics and Astronomy, State University of New York, Stony Brook, New York 11794-3800, USA*
[28]*Department of Physics, Tokyo University of Science, Noda, Chiba 278-0022, Japan*
[29]*Kamioka Observatory, Institute for Cosmic Ray Research, University of Tokyo, Kamioka, Gifu 506-1205, Japan*
[30]*Research Center for Cosmic Neutrinos, Institute for Cosmic Ray
Research, University of Tokyo, Kashiwa, Chiba 277-8582, Japan*
[31]*TRIUMF, Vancouver, British Columbia V6T 2A3, Canada*
[32]*Instituto de Física Corpuscular, E-46071 Valencia, Spain*
[33]*Department of Physics, University of Washington, Seattle, Washington 98195-1560, USA*
[34]*Institute of Experimental Physics, Warsaw University, 00-681 Warsaw, Poland*
(Dated: July 24, 2006)

The weak nucleon axial-vector form factor for quasi-elastic interactions is determined using neutrino interaction data from the K2K Scintillating Fiber detector in the neutrino beam at KEK. More than 12,000 events are analyzed, of which half are charged-current quasi-elastic interactions $\nu_\mu n \to \mu^- p$ occurring primarily in oxygen nuclei. We use a relativistic Fermi gas model for oxygen and assume the form factor is approximately a dipole with one parameter, the axial vector mass M_A, and fit to the shape of the distribution of the square of the momentum transfer from the nucleon to the nucleus. Our best fit result for $M_A = 1.20 \pm 0.12$ GeV. Furthermore, this analysis includes updated vector form factors from recent electron scattering experiments and a discussion of the effects of the nucleon momentum on the shape of the fitted distributions.

I. INTRODUCTION

The structure of the nucleon, as measured both by electrons and neutrinos, has been a subject of experimental study for decades. The discovery of neutrino oscillation and the availability of high precision electron scattering measurements have renewed interest in the study of neutrino interactions on nuclei. Neutrinos offer unique information about the structure of the nucleon and the nucleus. There are many experimental neutrino programs now running, under construction, or being planned for the near future, all of which use nuclear targets such as oxygen, carbon, aluminum, argon, or iron. Likewise, there has been significant progress in the calculation of cross sections, nuclear corrections, and backgrounds to specific processes. Improvement of these models, supported by neutrino data, will be important for the upcoming precision neutrino oscillation studies.

In this study we analyze distributions of the square of the four-momentum transfer $Q^2 = -q^2 = -(p_\mu - p_\nu)^2$ reconstructed from neutrino-oxygen interactions, where p_μ and p_ν are the momenta for the outgoing muon and incident neutrino. Using data from the Scintillating Fiber (SciFi) detector in the KEK accelerator to Kamioka (K2K) neutrino beam, we fit for the value of the axial vector mass M_A, the single parameter in the axial vector form factor (assuming a dipole form) for quasi-elastic (QE) interactions. For QE interactions, this parameter is obtained only from neutrino-nucleus scattering experiments. This is the first such measurement for oxygen nuclei, and we include a discussion of the effects of the oxygen nucleus and nucleon momentum distribution on the shape of the Q^2 distribution.

In the next section we briefly discuss the quasi-elastic form factors as well as list the cross-sections for non-quasi-elastic processes and nuclear effects. Then a section describes the K2K experiment, the neutrino beam, and the SciFi detector, including the detector performance. Following that are sections on the analysis technique, and the results, which include detailed discussion of the major systematic effects.

II. CROSS SECTION AND FORM FACTOR EXPRESSIONS

A. Quasi-elastic cross section

The differential cross section $d\sigma/dq^2$ for neutrino quasi-elastic scattering ($\nu_\mu\, n \to \mu^-\, p$) is described in terms of the vector, axial-vector, and pseudo-scalar form factors. The differential cross section[1] is written as:

$$\frac{d\sigma^\nu}{dq^2} = \frac{M^2 G_F^2 \cos^2\theta_c}{8\pi E_\nu^2} \times \qquad (1)$$
$$\left[A(q^2) - B(q^2)\frac{s-u}{M^2} + C(q^2)\frac{(s-u)^2}{M^4} \right]$$

where, s and u are Mandelstam variables, (s-u) $= 4ME_\nu + q^2 - m^2$, m is the outgoing lepton mass, M is the target nucleon mass, and E_ν is the neutrino energy. $A(q^2)$, $B(q^2)$, and $C(q^2)$ are:

$$A(q^2) = \frac{m^2 - q^2}{4M^2}\left[(4 - \frac{q^2}{M^2})|F_A|^2 \right.$$
$$-(4 + \frac{q^2}{M^2})|F_V^1|^2 - \frac{q^2}{M^2}|\xi F_V^2|^2(1 + \frac{q^2}{4M^2})$$
$$\left. -\frac{4q^2 F_V^1 \xi F_V^2}{M^2} - \frac{m^2}{M^2}((F_V^1 + \xi F_V^2)^2 + |F_A|^2) \right],$$
$$B(q^2) = \frac{q^2}{M^2}((F_V^1 + \xi F_V^2)F_A),$$
$$C(q^2) = \frac{1}{4}\left(|F_A|^2 + |F_V^1|^2 - \frac{q^2}{4M^2}|\xi F_V^2|^2 \right). \qquad (2)$$

In these expressions, the pseudo-scalar form factor F_P is negligible for muon neutrino scattering away from the muon production threshold and is not included. F_A is the axial vector form factor we will extract from the data. $F_V^1(q^2)$ and $F_V^2(q^2)$ are the Dirac electromagnetic isovector form factor and the Pauli electromagnetic isovector form factor, respectively. These formulas also assume the conserved vector current (CVC) hypothesis, which allows us to write F_V^1 and F_V^2 in terms of the well measured

*Now at University of Minnesota, Duluth

Sachs form factors G_E^P, G_E^N, G_M^P, and G_M^N:

$$F_V^1(q^2) = (1 - \frac{q^2}{4M^2})^{-1} \Big[(G_E^P(q^2) - G_E^N(q^2))$$
$$- \frac{q^2}{4M^2}(G_M^P(q^2) - G_M^N(q^2)) \Big],$$
$$\xi F_V^2(q^2) = (1 - \frac{q^2}{4M^2})^{-1} \big[(G_M^P(q^2) - G_M^N(q^2))$$
$$- (G_E^P(q^2) - G_E^N(q^2)) \big] . \quad (3)$$

In this paper we use the updated measurements of the Sachs form factors from [2, 3]. These new form factors have a significant effect on the extraction of F_A, compared to the previous dipole approximations. For the range of Q^2 of interest in this experiment, the updated values differ from the old form factors by up to $\pm$ 10%. We present results with both the new and the old form factors in this paper.

We approximate the axial vector form factor F_A as a dipole

$$F_A(q^2) = -\frac{1.2720}{(1 - (q^2/M_A^2))^2}, \quad (4)$$

which has a single free parameter, the axial vector mass M_A. Previous studies show that this approximation is reasonable [4–6]. The constant $F_A(q^2{=}0) = g_A/g_V = 1.2720\pm0.0018$ is determined from neutron decay measurements[7]. Because the Sachs form factors and other constants are precisely measured, the single parameter M_A can be determined from quasi-elastic neutrino interaction data.

B. Other cross sections

For this analysis, approximately half of the data comes from non quasi-elastic interactions, especially single pion events from the production and decay of the N^* and Δ baryon resonances within the nucleus. This background is described by the NEUT neutrino interaction Monte Carlo simulation [8] used by the K2K and Super-Kamiokande experiments. The resonance single pion events are from the model of Rein and Sehgal[9]. Our implementation includes contributions from eighteen resonances, of which three dominate the cross section. A comparison of this implementation with other neutrino event generators is given in [10].

Additional backgrounds, less important for our beam energy around 1.2 GeV, are also included. Deep inelastic scattering is from GRV94[11] for the nuclear structure functions with a correction described by Bodek and Yang[12]. The software PYTHIA/JetSet[13] is used to generate these events. This analysis takes the charged current coherent pion cross section to be zero following [14], and include neutral current coherent pion interactions as in Rein and Sehgal[15].

C. Nuclear Effects

Equation 1 is the differential cross section for the *free* nucleon, and must be modified to account for the effects of a nucleon bound in a nucleus. In the SciFi detector, the fiducial mass fractions are 0.700 H_2O, 0.218 Al, 0.082 HC, with an error of ±0.004. Our neutrino interaction Monte Carlo treats the entire fiducial mass as if it was made of H_2O; for targets other than a proton in hydrogen, we use a uniform Fermi gas model with $k_f = 225$ MeV/c for the nucleon momentum and an effective binding energy of -27 MeV, which is appropriate for oxygen. The primary effect of this nucleon momentum distribution on the quasi-elastic events is a significant suppression at low Q^2 due to Pauli blocking and a smaller overall suppression of $\sim$2% for the entire Q^2 distribution. The Fermi gas model is also applied to the non quasi-elastic interactions.

In addition to cross section effects, there are final-state interactions. The nucleus will cause reinteraction or absorption of secondary pions and recoil protons and neutrons in the neutrino interaction final state. Our model for these reinteractions is described in [8] with references. This will affect the observed distribution of the number of tracks. The resulting μ^- is also affected by the Coulomb interaction as it leaves the nucleus, losing approximately 3 MeV, though this effect is implicitly included in the Fermi gas parameters. The above nuclear effects are discussed quantitatively in the results section.

III. EXPERIMENT

A. The beam and detectors

The KEK to Kamioka (K2K)[16–18] experiment is a long baseline neutrino oscillation measurement in which a beam of neutrinos is sent from the KEK accelerator in Tsukuba, Japan to the underground Super-Kamiokande detector[19]. The neutrinos pass through a set of near neutrino detectors 300 meters from the target, after which they travel 250 km to Super-Kamiokande. The analysis in this paper considers only neutrino interactions detected in the Scintillating Fiber (SciFi) detector, one of the near detectors.

The wide-band neutrino beam at KEK is produced when 12 GeV protons hit an aluminum target. Two magnetic horns focus positively charged pions and kaons into a 200 meter long decay pipe, where they decay to μ^+ and ν_μ. The μ^+ are absorbed by the beam dump plus approximately 100 meters of earth between the decay pipe and near detector hall. The resulting neutrino energy is between 0.3 and 5 GeV and peaks at 1.2 GeV. The contamination in this beam includes 1.3% ν_e and 0.5% anti-ν_μ, estimated from a Monte Carlo simulation of the beam.

The near detector hall of the K2K experiment contains several detectors, shown in Fig. 1. The first detector

in the beam is the one-kiloton water Cerenkov detector. This study uses data from the SciFi detector, which is described in detail below. Following SciFi is the location of the lead glass detector which was used to measure the ν_e contamination in the beam. The lead glass detector was removed in 2002 and in its place was a prototype for a plastic scintillator (SciBar) detector. Then in 2003, the full SciBar detector [20] was installed, though data from this last running period is not used in the present analysis. Finally, there is a muon range detector (MRD) [21] which is used to estimate the momentum of the muons which escape the SciFi detector from charged current neutrino interactions. The MRD is also used to monitor the stability of the neutrino beam.
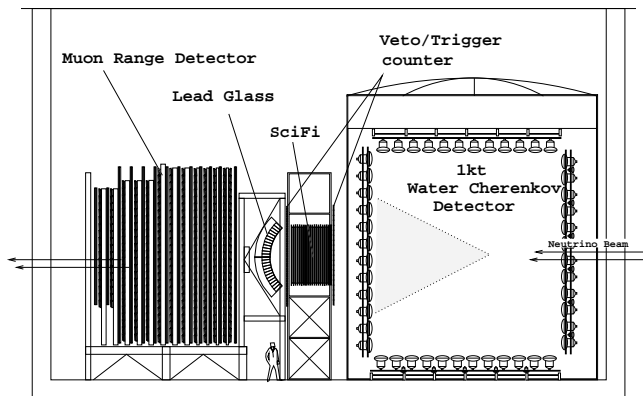

FIG. 1: The arrangement of the near neutrino detectors at KEK. The beam comes in from the right and continues to Super-Kamiokande, 250 km away to the left. The SciFi detector in on a stand in the middle.

The prediction for the shape of the neutrino energy spectrum of the K2K beam has significant uncertainty, up to 20% at higher energies. This prediction uses a Sanford-Wang parameterization of hadron production data and is verified using pion monitors downstream from the target[16]. This energy spectrum is measured using data from the near detectors and is used as input to the oscillation analysis [18]. The energy spectrum analysis is a simultaneous fit to the muon momentum and muon angle distributions from charged current interactions in the one-kiloton water Cerenkov detector, the SciFi detector, and the SciBar detector. The free parameters in this fit are a scale factor for the flux in eight energy regions, a scale factor for non quasi-elastic events, and many systematic error parameters specific to each detector. For this paper, we will refer to the above procedure as the neutrino energy spectrum measurement, and it defines the baseline Monte Carlo prediction for the SciFi detector data, prior to any fitting for the axial-vector mass, and is used throughout the discussion and plots in this Sec. III. This default MC simulation also uses zero charged current coherent pion and $M_A^{QE} = 1.1$ GeV. The

resonance single-pion cross section also involves its own axial-vector term with its own $M_A^{1\pi} = 1.1$ GeV. The analysis described in Sec. IV and V is mostly independent from the energy spectrum analysis, but uses a similar strategy.

B. The SciFi detector

The SciFi detector [22, 23] consists of scintillating fiber tracking layers between aluminum tanks filled with water. A schematic diagram is included in Fig. 2. There are a total of twenty 240 cm x 240 cm wide tracking layers, each of which consists of fibers oriented to give the particle location in the horizontal and vertical direction. These fibers are glued, one layer on each side, to a honeycomb panel which is 260 cm square. The distance between two tracking layers is 9 cm. Between the first and the twentieth layer are nineteen layers of aluminum tanks whose walls are 0.18 cm thick with an interior thickness 6 cm filled with water.
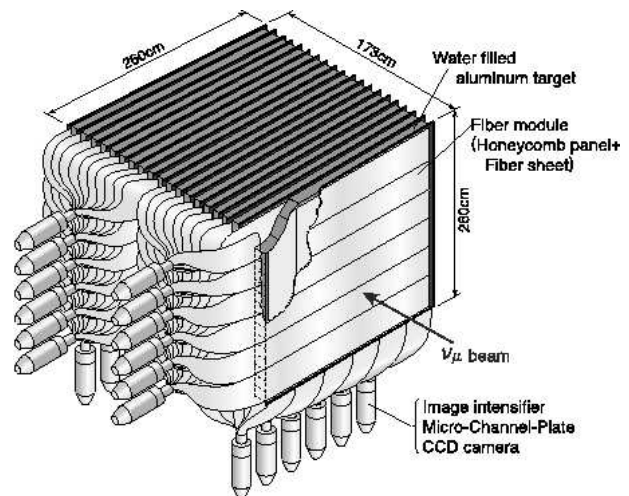

FIG. 2: A schematic diagram of the SciFi detector.

The scintillating fibers have a diameter of 0.7 mm and are read out by coupling them to image intensifier tubes and CCD cameras. The image intensifier preserves the position information of the original photo-electron. At the final stage, the light is recorded by a CCD camera. A total of 24 of these are used to read out 274,080 scintillating fibers. To reconstruct which fibers were hit, a one-to-one correspondence between the fibers and the position of pixels on the CCD camera is obtained from periodic calibration using an electro-luminescent plate.

To select charged-current events for this analysis, we require at least one track start in the SciFi fiducial volume and extend to, and stop within, the MRD. The fiducial volume has a mass of 5590 kg, includes the first through 17th tanks of water, and the reconstructed vertex must be within 110 cm from the center of SciFi in horizontal and vertical directions.

This requirement means that all events selected for this analysis have hits in at least three tracking layers of SciFi. There are also upstream and downstream scintillator hodoscopes which are read out by photo-multiplier tubes; we require a matching hit downstream and no hit upstream. This allows us to veto the small number of muons which come from in-time muon generation in the rock and upstream material in the detector hall, and also muons surviving from the target. Cosmic ray muons are suppressed by the beam timing requirement and are also negligible.

Tracks are reconstructed in the horizontal and vertical projections separately and then matched. The efficiency for reconstructing muon tracks with hits in three SciFi tracking layers is ∼70%, and rises to nearly 100% for tracks that penetrate five or more layers. Second tracks are required to produce hits in at least three SciFi layers, but there is no restriction on the maximum length.

Prior to 2002, all muons from SciFi are required to pass through and produce hits in segments of the lead glass detector, and these segments must match the location of the reconstructed track seen in SciFi and the MRD. On average, they deposit around 0.4 GeV of energy in the lead glass, though only path length, and not pulse size, is used to estimate the energy loss in this case. In the K2K-II run period, muons traveling through the SciBar prototype lose around 0.023 GeV of energy, though we do not require the track to pass through this detector. Muons traveling through many layers in SciFi deposit up to 0.3 GeV of energy.

The Muon Range Detector is made of alternating layers of drift tubes and iron plates; the first detection layer is upstream of the first piece of iron. The first four layers have a thickness equivalent to about 0.14 GeV of energy loss each, and the remaining layers are twice as thick. The muon momentum can then be estimated by calculating the muon's range from the interaction vertex.

C.   Data samples

The data for this analysis are obtained from two running periods between November 1999 and June 2003. The primary distinction between them is the configuration of the Super-Kamiokande detector, though there were simultaneous changes in the near detector configuration important for this analysis. We refer to the first as the "K2K-I" period; muons from neutrino interactions in SciFi pass through the lead glass detector on their way to the MRD. For these data, we accept muons which penetrate as little as one MRD detection layer, which corresponds to a muon momentum threshold of 675 MeV/c. The second running period is called "K2K-IIa" and has the prototype for the plastic scintillator detector SciBar [20] in place of the lead glass. For K2K-IIa, we require that the muons produce hits in the first *two* layers of the MRD, which gives a threshold of 550 MeV/c, in order to reduce the contamination from pions reaching the MRD.

Data from the continuation of the K2K-II period are not used in this analysis. In all cases, we require the muon not exit the MRD, which results in a maximum muon momentum of 3.5 GeV/c.

When two tracks reach the MRD, the longest, most penetrating track is assumed to be the muon. We have estimated using the MC that approximately 2% of these longest tracks are not the muon track. This is roughly 0.5% of the total sample. In the whole sample, another 0.5% of events were from neutral current interactions which had no muon at all.

This analysis uses only one-track and two-track events. Since quasi-elastic interactions will not produce such events, the 3% of events with three or more reconstructed tracks are discarded. For one-track events, the recoil proton or a pion is absent or below threshold. The requirement of three layers for the second track corresponds to a threshold of 600 MeV/c proton momentum and 200 MeV/c pion momentum.

The MC simulation includes the rescattering of protons, neutrons, pions, and other hadrons from the neutrino interaction final state as they leave the nucleus. The models for these final state interactions give good agreement with the number of tracks seen in SciFi, shown in Table I. Our estimate of the uncertainty in the number of two-track events due to the efficiency for finding the second track is 5%, which translates into ± 100 events for the K2K-I two-track sample. These events primarily migrate to or from the one-track sample. The extreme case of zero nuclear final state interactions in the neutrino interaction MC leads to 20% more events in the two-track category [24]. Further discussion of these effects can be found in Sec. V of this paper.

sample	1-track	2-track	3-track
K2K-I Data	5933	2181	187
K2K-I MC	5920	2176	203
K2K-IIa Data	3623	1344	148
K2K-IIa MC	3583	1396	136

TABLE I: Comparison between data and MC simulation of the number of reconstructed tracks observed in the SciFi detector for the K2K-I and K2K-IIa data samples. The MC is normalized to have the same number of events as the data. The estimated error in the number of two-track events due to tracking efficiency in reconstructing short, second tracks is 5%.

For two-track events, we separate quasi-elastic from non quasi-elastic events. Quasi-elastic interactions are a two-particle scattering process; the measurement of the muon momentum and angle is sufficient information to predict the angle of the recoil proton. If the measured second track agrees with this prediction within 25°, it is likely a QE event. If it disagrees, then it becomes a part of the non-QE sample. This is shown in Fig. 3, where the inset diagram demonstrates the kinematic quantity $\Delta\theta =$ angle between predicted and measured second track angle with respect to the beam. The quantity $\Delta\theta$ is plotted in
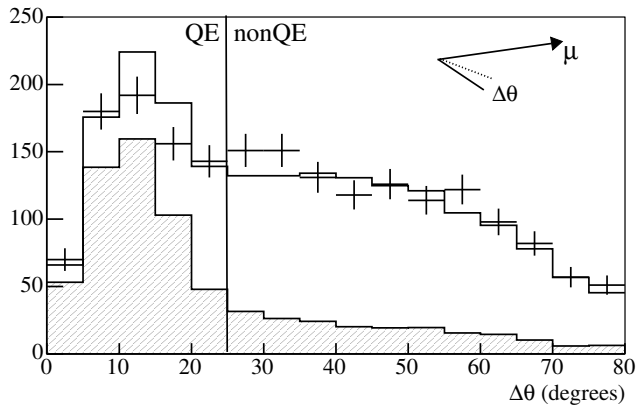
FIG. 3: The distribution of $\Delta\theta$, the difference between the predicted second track angle and the observed angle for K2K-I data. The histogram shows the Monte Carlo prediction, while the hatched region shows the QE fraction. In this analysis, $\Delta\theta = 25$ degrees is used to separate a QE enhanced sample. The inset diagram shows the definition of $\Delta\theta$.

this figure with the data and the baseline MC normalized to the data.

The value for this $\Delta\theta$ cut is chosen to give good separation between the QE and nonQE enhanced samples. We used the Monte Carlo simulation to estimate the efficiency for detecting the QE events, after all the cuts described above. Also we have estimated the purity of each sub-sample. These are shown in Table II. After these cuts, the total number of events in each sample is given in Table III.

	1-track	2-track		Total
		QE	nonQE	
K2K-I	35 (63)	5 (63)	2 (17)	42
K2K-IIa	38 (61)	5 (61)	2 (15)	45

TABLE II: Total reconstruction efficiency [%] for quasi-elastic interactions in each data set, the portion of efficiency from each sub-sample, and the QE purity of each sample (in parenthesis, [%]), estimated with the MC simulation.

	K2K-I		K2K-IIa	
	$Q^2 > 0.0$	$Q^2 > 0.2$	$Q^2 > 0.0$	$Q^2 > 0.2$
1 track	5933	2864	3623	1659
2 track QE	740	657	451	388
2 track nonQE	1441	789	893	478
Total	8114	4310	4967	2525

TABLE III: Number of events in three event samples and two data periods for the SciFi detector. Only events with reconstructed $Q^2 > 0.2$ (GeV/c)^2 are used for this M_A measurement, and are shown in separate columns and described in Sec. IV.

D. Muon momentum and angle distributions

An example of the muon momentum and muon angle distributions for the K2K-I data along with the Monte Carlo prediction are shown in Fig. 4 and Fig. 5. The MC distribution is normalized to the same number of events.
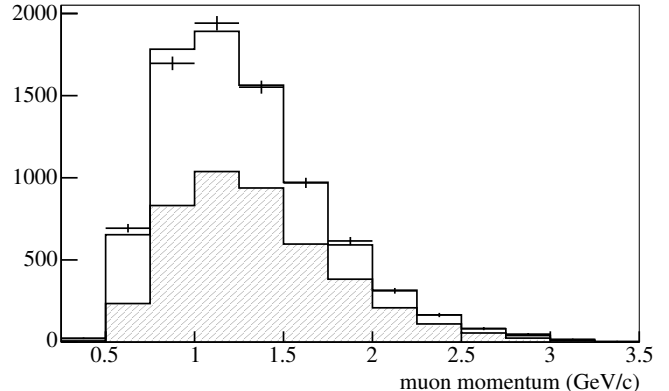

FIG. 4: Muon momentum distribution for all K2K-1 one-track and two-track events. The QE fraction, estimated from the MC simulation, is shown as the shaded region. The errors on the data are statistical only.

The yield of events with a muon at angles near the direction of the beam is particularly difficult to model in our Monte Carlo simulation; this is also discussed in [18]. A discrepancy was observed in all K2K near detectors,
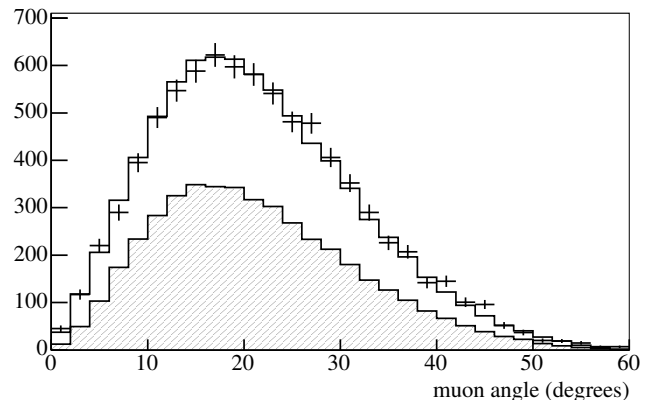
FIG. 5: Muon angle distribution for all K2K-I one-track and two-track events. The QE fraction, estimated from the MC simulation, is shown as the shaded region. Only statistical errors are shown.

including SciFi, and is presumed to be from some aspect of the neutrino interaction model.

The analysis of data from the SciBar detector [14] indicates that good agreement is achieved if our simulation has zero CC coherent pion production, and Fig. 5 uses this assumption. An example of the size of the effect on SciFi data is shown in Fig. 6. These are the same data

and MC as in Fig. 5, divided into the three standard sub-samples, but we have added the MC simulation including a prediction for CC coherent pion events shown with a dotted line. The MC distribution with zero CC coherent pion is normalized to the same number of events in the combined sample.

IV.   ANALYSIS

A.   Calculating Q^2 and E_ν

The kinematics the longest track in our events, which is assumed to be the muon, are sufficient to estimate the energy of the neutrino E_ν^{rec} and the square of the momentum transfer Q_{rec}^2, if the interaction is quasi-elastic.

$$E_\nu^{rec} = \frac{(m_N + \epsilon_B)E_\mu - (2m_N\epsilon_B + \epsilon_B^2 + m_\mu^2)/2}{m_N + \epsilon_B - E_\mu + p_\mu \cos\theta_\mu}, \quad (5)$$

$$Q_{rec}^2 = -q^2 = -2E_\nu(E_\mu - p_\mu \cos\theta_\mu) + m_\mu^2. \quad (6)$$

Here, E_μ and p_μ are the energy and momentum of the muon determined from the range, θ_μ is the angle relative to the beam direction, determined from the hits in the SciFi detector. Note that E_ν appears in the expression for Q_{rec}^2, and here we use E_ν^{rec}. The quantity $\epsilon_B = -27$ MeV for oxygen is the effective binding energy parameter from the Fermi gas model. The masses m_N and m_μ are for the nucleon and the muon. The resolution for E_μ is 0.12 GeV, due mainly to the MRD segmentation. The resolution for θ_μ is about 1 degree, but there is a tail to this distribution. The resulting value for E_ν resolution (for QE events) is 0.16 GeV and the resolution for Q^2 is 0.05 (GeV/c)^2 also with a tail coming from the measured angle. Finally, this formula assumes that the target neutron inside the nucleus is at rest, ignoring the nucleon momentum distribution for the event reconstruction. Fluctuations due to Fermi motion are about half the size of those due to detector and reconstruction effects, and contribute only a small amount to the reconstructed energy resolution.

It is important to note that these formulas are used for all events even though half the interactions are not quasi-elastic, because we do not identify the interaction mode on an event-by-event basis, nor is our beam at a fixed energy. The reconstructed E_ν and Q^2 are systematically off for these non quasi-elastic events: E_ν^{rec} is low by ∼0.4 GeV and Q_{rec}^2 is low by ∼0.05 (GeV/c)^2. However, all events are treated the same way, both data and Monte Carlo events. Thus, the comparison of data and MC in the fit is valid, but the distributions of the reconstructed values are affected by the non quasi-elastic fraction.

B.   Fit procedure

After calculating E_ν^{rec} and Q_{rec}^2 for each event, the data are binned in five E_ν^{rec} bins: 0.5 to 1.0, 1.0 to 1.5, 1.5 to 2.0, 2.0 to 2.5, and greater than 2.5 GeV. The data are divided into Q^2 bins each of width 0.1 (GeV/c)^2. To ensure there are usually five or more events in each bin, the smaller number of events at higher Q^2 are combined into a single bin. Despite the binning, some of these combined bins still have fewer than five events; this has a negligible effect on the fit values or the goodness of fit reported for this binning.

E_ν^{rec} (GeV)	0.5-1.0	1.0-1.5	1.5-2.0	2.0-2.5	>2.5
K2K-I 1-track	0.6*	1.1*	1.5	1.5	1.5
K2K-I 2-tk QE	0.5*	1.0*	1.3	1.3	1.3
K2K-I 2-tk nonQE	0.5	1.0*	1.1	1.1	1.1
K2K-II 1-track	0.6*	0.8	1.2*	1.2	0.9
K2K-II 2-tk QE	0.5*	1.1*	1.1*	1.1	1.1
K2K-II 2-tk nonQE	0.5*	0.8	0.9	0.9	0.9

TABLE IV: The low edge of the combined high Q^2 bin in (GeV/c)^2 for each subsample. The high Q^2 data were combined to ensure there are usually five events in each bin. The entries marked with an * still had fewer than five data events in the combined bin.

The expectation for the number of the events in each bin is computed from the Monte Carlo simulation for different values of the axial-vector mass and some systematic error parameters. We perform a maximum likelihood fit to the data by minimizing the negative of the logarithm of the likelihood which is based on Poisson statistics for each bin. In our case we use the modified form given in the Review of Particle Physics [7]

$$-2\ln\lambda(\theta) = 2\sum_{i=1}^{N}[\nu_i(\theta) - n_i + n_i\ln(n_i/\nu_i(\theta))] \quad (7)$$

in which $\nu_i(\theta)$ and n_i are the predicted and observed values in the i-th bin for some values of the parameters θ. The minimum of this function follows a chi-square distribution and can be used to estimate the goodness of the fit.

The expectation for each reconstructed E_ν and Q^2 bin is computed as follows:

$$N_{total}(n_{track}, E_\nu^{rec}, Q_{rec}^2) = A \left[N_{QE}(n_{track}, E_\nu^{rec}, Q_{rec}^2) \right.$$
$$\left. + R_{nonQE} \times N_{nonQE}(n_{track}, E_\nu^{rec}, Q_{rec}^2) \right] \quad (8)$$

where N_{QE} and N_{nonQE} are the separate contributions of quasi-elastic and non quasi-elastic events.

The free parameter A is the overall normalization. Five parameters $\Phi(E_\nu^{true})$, not included in the above expression, are used rescale the neutrino flux in each energy region, four of which are unconstrained in the fit, while the relative flux for energies from 1.0 GeV to 1.5 GeV is fixed at 1.0. The flux is reweighted based on the true
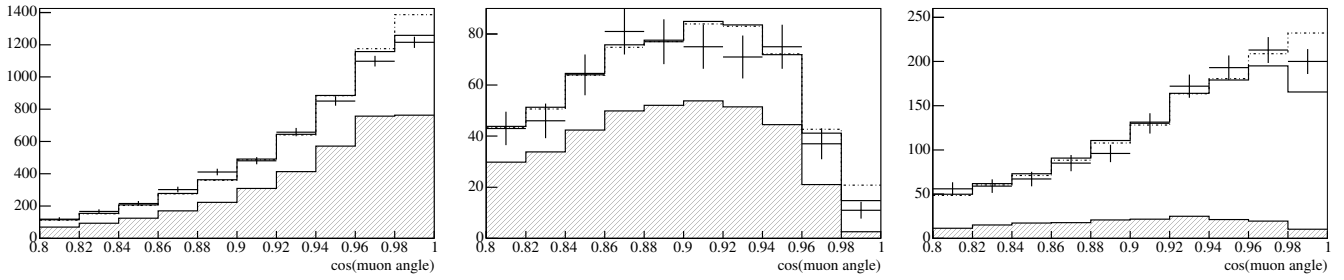
FIG. 6: Distribution of $\cos(\theta_\mu)$ for data and MC, showing the data at small angle, which is also the low Q^2. Left to right are the one-track, two-track QE enhanced, and two-track nonQE enhanced samples. The dashed line is with charged-current coherent pion, the solid line without. The shaded region is the QE fraction, estimated from the MC simulation. The distributions are normalized to the total number of events when all three samples are combined.

energy of the MC events, and applies to both QE and nonQE events. The nonQE background is reweighted using the unconstrained parameter R_{nonQE}: the relative reweighting of our default MC calculation. Because of the separation of the two-track QE and non-QE samples, the R_{nonQE} reweighting will be constrained by the background and allow a fit for the QE axial-vector form factor. The parameters A and R_{nonQE} are relative to the data/MC normalization calculated using all other parameters at their nominal values, including $M_A = 1.1$ GeV. Importantly, changing the value for M_A^{QE} changes the absolute cross-section for QE, which will in turn affect the fit value for the free R_{nonQE} parameter and the overall normalization.

In this expression, N_{QE} is based on a calculation of the quasi-elastic cross section with the free parameter M_A. This cross section is computed using the true energy and Q^2 and convoluted with the detailed shape of neutrino energy spectrum, flux(E), from the beam MC calculations and the hadron production parameterization used in [16].

$$
N_{QE}(n_{track}, E_\nu^{rec}, Q_{rec}^2) = \sum_{E_{true}, Q^2_{true}}^{\text{all bins}} \Big[\text{ flux}(E_\nu^{true})
$$
$$
\times \, d\sigma/dQ^2(E_\nu^{true}, Q_{true}^2, M_A) \, \times \, R(E_\nu^{true}, Q_{true}^2)
$$
$$
\times \, M(E_\nu^{true}, Q_{true}^2 \to n_{track}, E_\nu^{rec}, Q_{rec}^2) \Big]. \quad (9)
$$

Nuclear effects that modify the cross section, especially Pauli blocking and and other effects of the nucleon momentum distribution, are included using the factor R, and are discussed in Sec. V.

Because the cross section is calculated using true kinematics, it must be modified to account for detector acceptance and resolution, as well as nuclear final state interactions, in order to obtain the expectation in different reconstructed E_ν and Q^2 bins. This is done with a migration matrix M in the above equation where n_{track} refers to the one-track, two-track QE, and two-track non-QE samples. This matrix is computed directly from the Monte Carlo simulation. This result is then applied to

the calculated cross section to determine the number of QE events in each reconstructed E_ν and Q^2 bin. In contrast, the shape of the non-QE background is taken directly from the Monte Carlo simulation and already includes these effects.

The combination of four flux reweighting factors $\Phi(E_\nu)$ and the overall normalization are unconstrained. The parameter M_A itself affects the total cross-section as a function of energy. In this way, we are fitting the shape of the Q_{rec}^2 distribution separately *in each energy region*. This ensures that the axial mass measurement is not significantly biased by the normalization in any one energy bin.

Finally, the lowest Q_{rec}^2 bins, events below 0.2 $(\text{GeV/c})^2$, are not included in the fit. The low Q^2 region is where there is the largest uncertainty due to the model for nuclear effects, especially Pauli blocking. This eliminates almost half the data, and the total number of events actually included in the fit is shown in the second column for each data set in Table III. Low Q_{rec}^2 events are also events at low angle, shown by the $\cos(\theta)$ term in parenthesis in Eq. 6, and corresponds to the right-most two bins in the $\cos(\theta)$ histograms in Fig. 6 for neutrino energies around 1.0 GeV.

C. Fit Parameters

We fit a large collection of E_ν^{rec} and Q_{rec}^2 distributions: two data sets K2K-I and K2K-IIa, each with one-track, two-track QE, and two-track non-QE subsamples, a total of 242 bins. The Monte Carlo predictions for these data sets are computed separately using MC samples that are more than 15 times larger than the data. The free parameters Φ for the flux at each energy are common to both data sets, as is the overall normalization factor, the non-QE/QE ratio and proton rescattering. There are separate 2-track to 1-track migration parameters for each data set, ten parameters in total.

These last three parameters are constrained by adding a term to the chisquare. A reweighting or migration is computed and a systematic error for each of these, as-

sumed to be approximately Gaussian, is estimated from studies of the detector and interaction Monte Carlo simulations. As the fit is performed, a chisquare is evaluated, assuming this Gaussian shape and error, and is added to the total chisquare. The total degrees of freedom is thus $(242 + 3)$ chisquare terms - 10 parameters = 235 degrees of freedom.

Proton rescattering is taken to be uncertain by $\pm 20\%$ from the nominal value used in the NEUT Monte Carlo simulation. A reweighting of events is calculated from a second full-detector Monte Carlo simulation using 80% of the proton reinteraction cross sections, and the systematic error parameter is used to interpolate between these data samples. This reweighting has the primary effect of increasing or decreasing the number of QE events in the two-track sample, by up to +4.5% for the 80% case. The actual effect on the fit is to increase or decrease the number of events in the QE enhanced sample because only that part of the two-track sample has high QE purity.

The 2-track to 1-track migration is assigned a $\pm 5\%$ error. This error is based on the estimated error in the track-finding efficiency for short, second tracks. Because the detector response and tracking is tuned separately for the K2K-I and K2K-IIa data samples, we include separate parameters for each sample in our fit. This migration is applied to all events in the MC, not just the QE events as for proton rescattering. This parameter is also correlated with neutrino interaction effects such as proton and pion rescattering.

V. RESULTS AND DISCUSSION

A. Fit Results

The result of the combined fit is $M_A = 1.20 \pm 0.12$ GeV. The chisquare value for this fit is 261 for 235 degrees of freedom. The Q^2 distributions for the data and the MC simulation with the best fit M_A are shown in Fig. 7, with all five energy regions combined. The best fit values for the free parameters in the fit are summarized in Table V.

In the fit, there is a strong correlation between the normalization, R_{nonQE}, and the two-track to one-track migration, but different ways of constraining the parameters do not affect the fit value of M_A very much. The migration is expressed such that 0.90 means 10% of the two-track events in each E_{rec} and Q^2_{rec} bin should be moved to the corresponding one-track bin; this parameter is being pulled beyond its 5% gaussian constraint for both samples. For example, fixing the 2-track to 1-track migration at 0.95, the one-sigma edge of the 5% error, yields normalization = 0.975, $R_{nonQE} = 1.26$, and proton rescattering 1.20. However, M_A is unchanged while the chisquare rises to 261 for 234 degrees of freedom.

Finally, one further comment about the R_{nonQE} parameter. The higher fit value for M_A^{QE}=1.20 GeV causes an increase of about 10% in the absolute QE cross sec-

tion, relative to the default value of M_A^{QE}=1.10 GeV. If a good fit requires maintaining a similar relative non-QE cross-section, then a corresponding increase in R_{nonQE} parameter and decrease in the absolute normalization is required. This appears as a portion of the $R_{nonQE} = 1.30$ fit value and normalization.

parameter	fit value	error
M_A (GeV)	1.20	0.09
Φ(0.5 to 1.0 GeV)	1.02	0.25
Φ(1.0 to 1.5 GeV)	1.00	fixed
Φ(1.5 to 2.0 GeV)	0.80	0.09
Φ(2.0 to 2.5 GeV)	0.93	0.08
Φ(> 2.5 GeV)	1.09	0.11
Normalization	0.96	0.09
R_{nonQE}	1.30	0.17
K2K-I 2tk → 1tk	0.94	0.02
K2K-IIa 2tk → 1tk	0.94	0.03
Proton Rescattering	1.14	0.18

TABLE V: Best fit values for the parameters in the fit. The errors given are from the fit only. The error for M_A rises to ±0.12 GeV when the other systematic effects are included

B. Consistency checks

A test for consistency is to vary the low Q^2 cut and compare the results. In Fig. 8, the best fit M_A is shown with different minimum Q^2_{rec}. This is done with identical fit conditions and free parameters as described above; the systematic error parameters are still allowed to vary in these fits. The error bars include an estimate of statistical errors only; however, the data for each point in this figure are correlated with the other points. The extra error bar shows the total error. When no cut is applied (and no coherent pion), the fit value is $M_A = 1.27 \pm 0.12$ GeV. In this case, the combination of errors reported in the regular fit falls to ± 0.09 GeV mostly because of the increased size of the sample used in the fit, but we estimate a large additional systematic error of ± 0.07 GeV should be included (but not shown in Fig. 8) due to uncertainty in the amount of Pauli blocking. The fit values are all higher than the best fit as the minimum Q^2 cut eliminates the higher statistics, low Q^2 portion of the data. When only the higher Q^2 regions are included in the fit, the shape of the Q^2 spectrum is systematically flatter and preferrs a higher M_A. When the systematic errors are considered, these results are consistent with the full fit value.

A third check is to consider the fit values for the Q^2 distribution *at each energy*, shown in Fig. 9. This uses the best fit values for the flux for all energies except the one being tested while the chisquare, and therefore the shape fit, is computed only for the energy bins in question. This is necessary because of the significant migration from true energy (where the flux parameter is applied) to reconstructed energy used in the fit, especially for the non-QE background. It also has the consequence
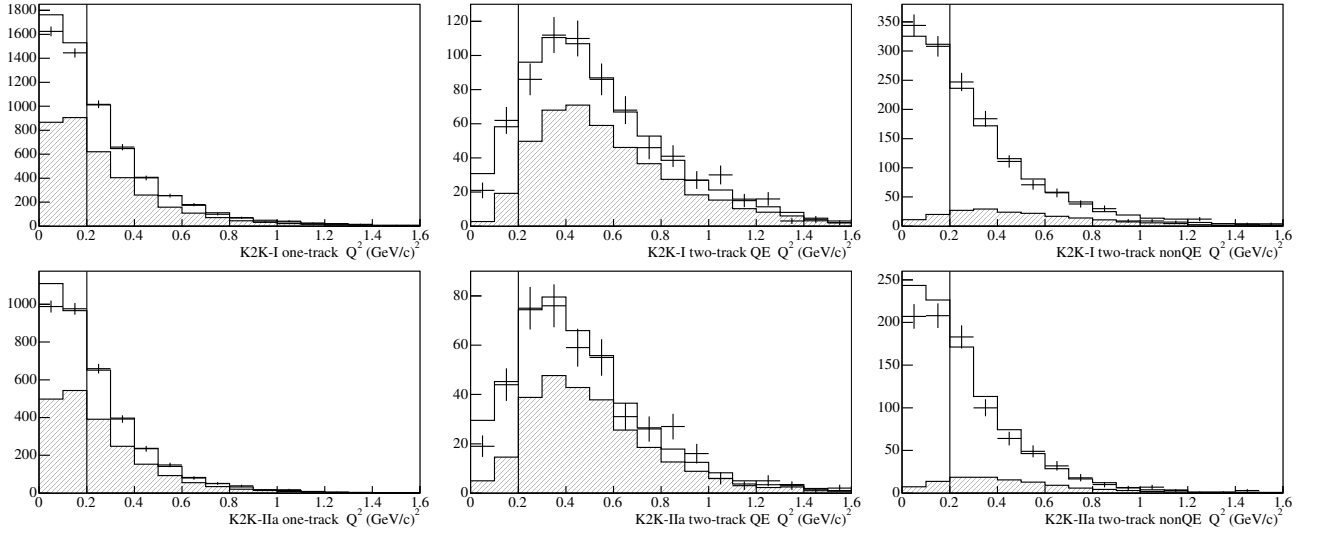
FIG. 7: The data and the best fit Q^2_{rec} distributions for K2K-1 data (top) and K2K-IIa data (bottom) for the 1-track, 2-track QE enhanced, and 2-track non-QE enhanced samples. The shaded region shows the QE fraction of each sample, estimated from the MC. The contribution from each energy region is summed for each plot. The lowest two data points in each plot are not included in the fit, due to the large uncertainty in the effects of the nucleus.
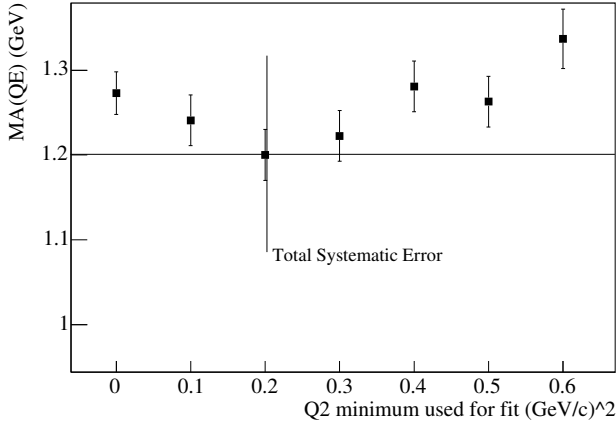

FIG. 8: Fit values obtained for different values of the low Q^2 cut. Only statistical errors are shown. The horizontal line is the combined best fit. The vertical line is the systematic errors.

this result should not be considered a measurement, but rather a consistency test. However results for each energy are also consistent with the combined result.
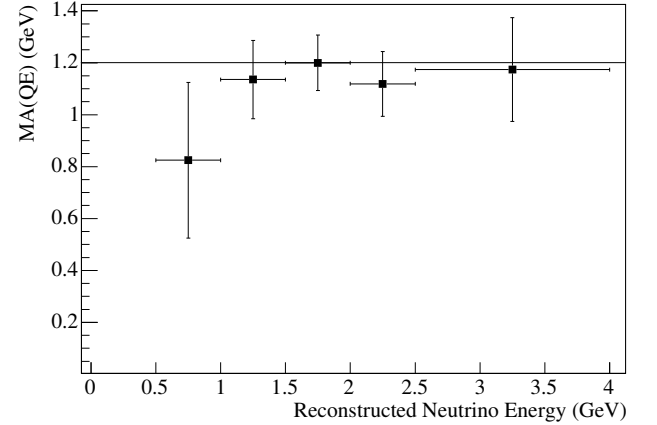

FIG. 9: Fit values obtained separately from the shape of the Q^2 distribution for each neutrino energy. The horizontal line indicates the combined best fit value.

that these data points are correlated. This again causes the feature that the fit points are not symmetric around the full fit value; they are the same or lower. The dominant reason is the unconstrained parameter for the flux in the one energy region being tested while the others are held fixed at the full-fit values. If the flux in that one energy region was also held fixed, the middle point (the one whose data dominates the fit) does move to higher value of M_A. The resulting plot roughly retains the features while becoming more symmetric around the full fit point. Overall, there are different systematic effects, and

Finally, we fit for the value of M_A for the K2K-I and K2K-IIa data sets separately, and obtain the values 1.12 $\pm$ 0.12 (χ^2 150/127 dof) and 1.25 $\pm$ 0.18 GeV ($\chi^2 =$ 109/101 dof) respectively. The primary difference between the two data sets are the presence or absence of the lead glass detector and the accompanying uncertainty in the muon momentum scale. Also, the muon thresholds are somewhat different, and the acceptance model for short, second tracks in SciFi is calibrated separately

for the two data sets, which could show up in the 2-track to 1-track migration.

C. Systematic uncertainties

Here these systematic errors are discussed in detail. The largest contributions to the systematic error, summarized in Table VI, are the uncertainty in the muon momentum scale, and the normalization and uncertainty in the flux for each energy region. Other, smaller contributions include the shape of the non-QE background, the non-QE/QE ratio, and the two-track to one-track migration. A final, interesting source of uncertainty comes from nuclear effects, though it contributes only a small amount to this analysis. The statistical error is estimated by setting all the other parameters in the fit to their best fit values and determining the resulting error in M_A, though there is a further statistical effect in the normalization parameter.

Sources of uncertainty	Error in MA
Muon momentum scale	0.07
Relative Flux and normalization	0.06
M_A 1-π	0.03
R_{nonQE}	0.03
Proton rescattering	0.03
Statistics	0.03
Total	0.12

TABLE VI: The calculation of the total error. Errors smaller than 0.03 are not listed. The total value takes into account the correlations among those errors that are parameters in the M_A fit; the others are added to that total in quadrature.

1. Muon momentum scale

The muon momentum appears directly, and indirectly via E_ν, in the calculation of the value of Q^2_{rec} for each event. The uncertain absolute scale for this momentum, as modeled in the detector Monte Carlo simulation, will cause the MC prediction for the shape of the Q^2_{rec} distribution to be more or less compressed and affect the M_A measurement. As an example, a $\pm 1\%$ error in the momentum scale gives a ∓ 0.05 GeV error in the fit value for M_A. Approximately ∓ 0.01 GeV of this error can be attributed to shifting a small number of events up or down one E^{rec}_ν bin. The other ∓ 0.04 GeV is from the calculation of the reconstructed Q^2 itself. The central value for the muon momentum scale is determined from the neutrino energy spectrum analysis, described in Sec. III and reference[18], while the error from that analysis is propagated to the M_A analysis as described below.

Because the muon momentum is measured using its range in the detector, the uncertainty for the overall momentum may come from any of the pieces of the detector: SciFi, LG, SciBar, or the MRD. In this analysis,

we model this uncertainty by assigning it to just two of these. The first is the uncertainty in the density of the lead-glass detector and therefore the energy loss experienced by the muon passing through it. The second piece is a scaling factor for part of the muon momentum calculated from the range in the MRD detector. For both pieces, we determine the central value of the momentum shift and the error from the neutrino data.

The density of the lead glass, which is incorporated into the geometry description in our Monte Carlo simulation, is determined from a beam test and is uncertain by 5%. We have modeled the effect of this uncertainty and made a reweighting table that modifies the MC p_μ and θ_μ distribution. This uncertainty could give rise to a 2% error in the total momentum for a typical K2K-I event. In the neutrino energy spectrum measurement, this is a parameter in the fit and good agreement with the data is found with a value that is 0.98 ± 0.013 times the density obtained from the beam test; the neutrino data provide the stronger constraint. This central value is used in the M_A analysis.

Likewise, we measure a shift in the muon momentum scale for the Muon Range Detector of 0.976 ± 0.007 using the energy spectrum measurement procedure. When the K2K-I and K2K-IIa data are fit separately, we obtain a consistent result for this parameter, despite the presence of the lead glass detector in the former. This is assigned as an error for the MRD portion of the muon range, but it actually arises from a combination of factors including the material assay for the MRD and SciFi (about 1%), the simulation of muon energy loss in GEANT [25] (about 1%) and the uncertainty in the intrinsic muon momentum from the neutrino interaction MC (about 0.5%). Again, we find the neutrino data produce a good central value and a tighter constraint than taking the individual errors in quadrature. Though these errors actually come from all portions of the muon track, we find no significant difference in the analysis if this factor is obtained from and applied to the whole track momentum, instead of the MRD portion only.

Because the M_A fit and the energy spectrum analysis use the same neutrino data, it is possible that the uncertain value for M_A itself is affecting the fit values for the MRD muon momentum scale when that value is obtained from the spectrum measurement. Our default Monte Carlo assumes $M_A = 1.1$ GeV. An uncertainty in this value of ± 0.20 GeV corresponds to an error of ± 0.01 in the fit value of the momentum scale. This is taken as an additional uncertainty when this parameter is used to determine M_A. Also, there is a correlation between the lead-glass density error and the MRD momentum error. When all of these effects are combined, the resulting error in M_A is ± 0.07 GeV.

2. Flux for each energy region and normalization

A significant uncertainty in M_A arises because the relative neutrino flux for each energy region and the overall normalization parameters are unconstrained parameters in the fit. In this way we are fitting the shape of the Q^2 distribution in each energy region separately, regardless of the errors in the incident neutrino flux. The contribution to the total error is estimated by fixing the other free parameters in the fit and reading the resulting error in M_A, which is from these parameters and statistics only.

The overall normalization contributes more to the error than the uncertain relative normalization. This is estimated by further constraining the relative flux so that only the normalization and M_A are free. The overall normalization is correlated with M_A because M_A affects both the relative size of and the shape of the QE cross-section. Different combinations of M_A and normalization will give a reasonable chisquare when compared with the data, and the error due to this parameter, more than the others, would be reduced with increased data statistics, even with no further constraints. This last result is confirmed using MC samples of various sizes as if they were data, to study the effect of statistics of the data sample.

We do have a constraint on the relative flux for each energy region from the neutrino oscillation measurement [18]. This measurement is done using data from all the near detectors, not just SciFi. This information is not completely independent of this analysis because it shares some of the same data set, but a different analysis technique, and several other data sets from the other near detectors. We get a consistent result $M_A = 1.13 \pm 0.12$ GeV when this constraint is used.

3. R_{nonQE} parameter and two-track to one-track migration

The R_{nonQE} reweighting is also a free parameter in the axial-mass fit. There is no constraint on this parameter for this analysis, though other estimates find that it is uncertain by 5 to 10% [18]. The two-track to one-track migration parameter is highly correlated with R_{nonQE}, and when these two are combined, they contribute a total error of 0.03 GeV to the fit value of M_A. As before, this is obtained by fixing all the other parameters such that the resulting error in M_A is the combination of these and the statistical error only.

4. Non quasi-elastic background shape

Single pion events from the production and decay of the Δ and other resonances in the nucleus are the largest background to the QE samples in this analysis. These events are described by a calculation that includes a similar axial mass parameter which affects the shape of the Q^2 distribution. If the value used to model the single pion background is different, that will affect the fit value obtained for the quasi-elastic events. Our calculation takes $M_A^{1\pi} = 1.1 \pm 0.1$ GeV. This contributes an uncertainty of ∓ 0.03 to result for M_A^{QE}, and is estimated by generating a second complete MC sample with $M_A^{1\pi} = 1.2$ GeV.

Other contributions to the nonQE background are deep inelastic scattering and coherent pion production. For the former, we have evaluated the uncertainty by removing the Bodek-Yang correction, and find no effect. We also consider the case where charged-current coherent pion events are produced which has only $+0.01$ GeV effect for the $Q^2 > 0.2$ cut used in the standard analysis, but increases the fit value by 0.10 GeV when we fit the entire Q^2 range.

5. Nuclear effects

Other interesting sources of uncertainty are the effects of the nucleus on the cross section and the Q^2 distribution, primarily from the nucleon momentum distribution. The effects are small relative to the other uncertainties described above because the minimum Q^2_{rec} cut eliminates the data where these errors are most significant. These effects will be of interest for future precision experiments and as models of neutrino-nucleus interactions become more sophisticated. We present a description of these effects for the uniform Fermi gas model, in this case from the calculation in [26, 27]. The three effects are described below and summarized in Fig. 10 for a 1.0 GeV neutrino. It is the ratio in this figure that is the basis for $R(E_\nu, Q^2)$ in Eq. 8.

The main uncertainty is the amount of Pauli blocking that should be applied both to the quasi-elastic and also the single pion background. Within the context of the Fermi gas model, this can be estimated by assuming a different k_f: 215 and 235 in addition to the default value of 225 GeV/c. The effects of this uncertainty on M_A do not appear with the $Q^2 > 0.2$ requirement used in this analysis, but are as much as 5% for fits that use the lowest Q^2 events.

At the upper end of the Q^2 distribution, the quasi-elastic cross section has a kinematic cut off whose location depends on the incident neutrino energy. The momentum distribution in a nucleus smears this step, giving a tail to the distribution. These high Q^2 interactions produce muons that do not reach the MRD because they are at high angle or their momentum is too low, so this has no effect on the present analysis.

The momentum distribution will modify the shape of the Q^2 distribution through the middle region between the two effects described in the preceding paragraphs. The slope of the middle region in the second plot in Fig. 10 is approximately 0.017 $(GeV/c)^{-2}$. There is also an overall suppression of the cross section of 2%. The uncertainty represented by the change in slope can be propagated to the M_A analysis by modifying $R(E, Q^2)$ in the fit. The resulting uncertainty in M_A is ± 0.01 GeV, negligible
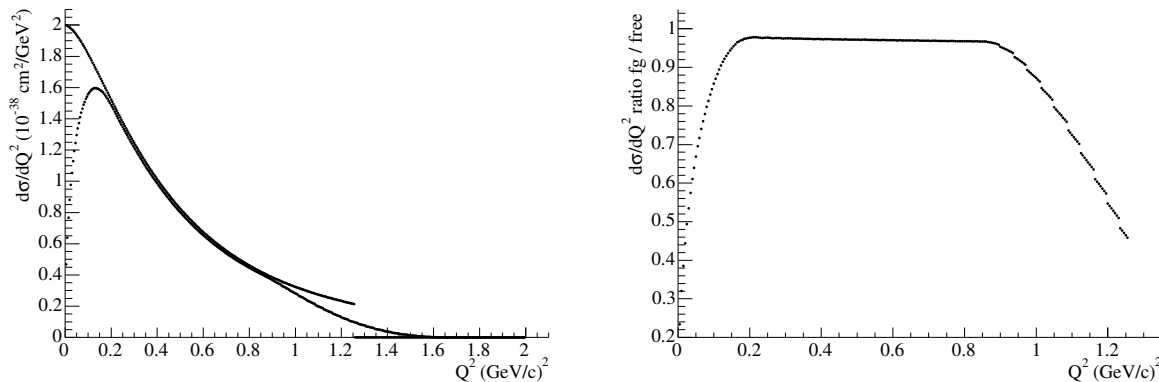
FIG. 10: Effect of the nucleon momentum on the shape of the Q^2 distribution. The comparison is between the free nucleon and a uniform Fermi gas model. The effect of Pauli blocking is seen at low Q^2, the tail of the momentum distribution at high Q^2, an overall suppression, and a slight change in the slope in the middle region. The calculated quasi-elastic cross sections for 1.0 GeV neutrinos on oxygen are on the left, and the ratio (Fermi gas)/ (free neutron).

compared to the other uncertainties in this analysis.

In addition to the estimate of the effects of the nucleus, this implies a conversion factor that may be used by the reader to evaluate small changes to the model, as long as they can be approximated by a shift in the slope of the Q^2 distribution as in the preceeding paragraph. Likewise, an adjustment of the slope of the non-QE background of 0.02 $(GeV/c)^{-2}$ relative to nominal will yield a ∓ 0.01 GeV shift in the fit value of the M_A^{QE}. A variety of corrections that yield a shift in M_A of up to 0.05 GeV are well reproduced by this approximation.

A final uncertainty from the nuclear model is the nucleon interaction energy. For our Fermi gas model, this takes the form of an effective binding energy -27 ± 3 MeV, and is the energy given up to the recoil proton from the nucleus. This affects the outgoing muon momentum and would contribute ± 0.02 GeV error to M_A, but this is naturally included by the free muon momentum scale parameter in this analysis.

These uncertainties are also used to estimate the effect of the 21.8% aluminum that makes up the fiducial mass. The neutrino-aluminum interactions are taken to have the same cross section per nucleon and the same kinematics as for oxygen. A higher k_f appropriate for aluminum only has an effect in the Pauli blocked region. The increased effective binding energy is equivalent to a shift in p_μ of about 3 MeV for this fraction of the interactions, and thus is negligible for the whole sample.

D. Effect of the new vector form factors

The basic method used to measure the axial vector mass here is the same as for previous measurements, listed in Table VII, but since that time there have been improved measurements for the shape of the vector form factors from electron scattering experiments. Changing

the shape of the contribution of the vector form factors affects the fit shape of the axial-vector form factor. We continue to assume F_A has a dipole form; future high-precision neutrino experiments may be sensitive to subtle differences from a F_A dipole shape.

Our results assume the updated parameterizations of Bosted [2]. We have evaluated one other recent parametrization [3] and found the M_A result differs by only 0.01 GeV. This is true even considering the discrepancy between the polarization transfer measurement and the Rosenbluth separation measurement, described in [3] with further references. For our analysis, we use the parameterization of G_E^N given by [34].

In order to allow comparison with the previous results, we have repeated the analysis with the same modified dipole approximations used by [4–6] who follow Olsson et al. [35]. We find that these old parameterizations produce a value that is 1.23, roughly 0.03 higher. When only a pure dipole is used, the fit value is 1.27 GeV.

E. Comparison with other experiments

This is the first measurement of the axial vector mass using neutrino interactions with oxygen targets, but there have been many previous measurements with a variety of other target nuclei. The experiments in Table VII have hundreds or thousands of events from neutrino or anti-neutrinos with energies of a few GeV. The systematic errors they report are dominated by uncertainties in the neutrino flux, calculation of nuclear effects, and subtraction of non-quasielastic backgrounds. These results are also reported, with some discussion, in the review article [36].

One significant difference between this analysis and many of the previous measurements in Table VII is the purity of the quasi elastic samples from which M_A is ob-

Experiment	Pub. Date	Target	Method	M_A	Error	comment
ANL [6]	1982	D	12' Bubble Chamber	1.00	± 0.05	
FNAL [5]	1983	D	15' Bubble Chamber	1.05	+0.12 - 0.16	
BNL [4]	1990	D	7' Bubble Chamber	1.07	+0.040 -0.045	
CERN [28]	1977	CF_3Br	GGM Bubble Chamber	0.94	± 0.17	
CERN [29]	1979	CF_3Br, C_3H_8	GGM Bubble Chamber	0.94	± 0.05	
SKAT [30]	1990	CF_3Br	Bubble Chamber	1.05	± 0.14	(ν)
SKAT [30]	1990	CF_3Br	Bubble Chamber	0.79	± 0.20	$(\bar{\nu})$
BNL [31]	1969	Fe	Segmented Tracker	1.05	± 0.20	
BNL [32]	1987	HC, Al	Segmented Tracker	1.06	± 0.05	elastic scattering
BNL [33]	1988	HC, Al	Segmented Tracker	1.09	± 0.04	$(\bar{\nu})$
K2K SciFi	this expt.	H_2O, Al	Segmented Tracker	1.27	± 0.12	dipole form factors

TABLE VII: Results from other experiments, grouped first by target nucleus, then by publication date. Where separate values are given for M_A extracted from the shape of $d\sigma/dQ^2$ only, that is the value included in this table. All the data are for the neutrino quasi-elastic reaction ($\nu\, n \to \mu^-\, p$) except for two which also took data with anti-neutrino ($\bar{\nu}\, p \to \mu^+\, n$), one of which studied neutral current (elastic) scattering, noted in the table. For better comparison with other experiments, the K2K SciFi result is the one analyzed with dipole vector form factors.

tained. The consistency check giving fit values for different choices of Q^2_{min} in Fig. 8 may be sensitive to this, as the sample purity increases when only high Q^2 events are considered. We have also checked the consistency as a function of the $\Delta\theta$ parameter that separates the two-track samples into QE enriched and non-QE subsamples. Choosing a smaller $\Delta\theta$ does not improve the purity, but a larger value reduces the purity of the two-track QE enriched subsample. A range of $\Delta\theta$ between 15 and 35 degrees produces less than ± 0.02 GeV effect on the fit value for M_A.

One other difficulty with comparing the results in Table VII is that the older analyses used not only different assumptions about the vector form factors, but also different backgrounds and other physical constants such as $F_A(q^2=0)$. The results given here are the published values; however, the authors of [3] have made some effort to reproduce and then update all of the analysis assumptions for a selection of these experiments.

VI. CONCLUSION

We have made the first measurement of the axial vector form factor using neutrino interactions on an oxygen target. We find an axial vector mass $M_A = 1.20 \pm 0.12$ GeV gives the best agreement with the data, if we assume a dipole form for F_A. This analysis includes the updated (non-dipole) vector form factors obtained from electron scattering experiments. In order to better compare with previous experiments, an alternate result using only pure dipole vector form factors is $M_A = 1.27 \pm 0.12$ GeV. This result is higher than previous measurements,

especially those on deuterium. We find the most significant sources of systematic error are experimental, and our results are different from deuterium measurements by about two standard deviations. We note that this analysis is very sensitive to the absolute muon momentum scale. We do not assume that neutrino interactions on oxygen should be the same as for deuterium. In this sense, we have measured the effective M_A for oxygen. However, we find only a small effect on the shape of the Q^2 distribution for $Q^2 > 0.2$ $(\text{GeV/c})^2$ from known nuclear effects.

[1] C. Llewellyn-Smith, Phys. Lett. C **3C** (1972).
[2] P. E. Bosted, Phys. Rev. C **51**, 409 (1995).
[3] H. Budd, A. Bodek, and J. Arrington, hep-ex/0308005 (2002).

[4] T. Kitagaki et al., Phys. Rev. D **42**, 1331 (1990).
[5] T. Kitagaki et al., Phys. Rev. D **28**, 436 (1983).
[6] K. Miller et al., Phys. Rev. D **26**, 537 (1982).
[7] S. Eidelman et al., Phys. Lett. B **592** (2004).
[8] Y. Hayato, Nucl. Phys. B Proc. Supp. **112**, 171 (2002).
[9] D. Rein and L. Seghal, Ann. Phys. **133**, 79 (1981).
[10] H. Gallagher et al., Nucl. Phys. B Proc. Supp. **139**, 278 (2005).
[11] M. Gluck, E. Reya, and A. Vogt, Z. Phys. C **67**, 433 (1995).
[12] A. Bodek and U. K. Yang, Nucl. Phys. B Proc. Supp. **112**, 70 (2002).
[13] T. Sjostrand, Comput. Phys. Commun. **82**, 74 (1994).
[14] M. Hasegawa et al., Phys. Rev. Lett. **95**, 252301 (2005).
[15] D. Rein and L. Seghal, Nucl. Phys. B **223**, 29 (1983).
[16] S. H. Ahn et al., Phys. Lett. B **511**, 178 (2001).
[17] M. H. Ahn et al., Phys. Rev. Let. **90**, 041801 (2003).
[18] E. Aliu et al., Phys. Rev. Lett. **94**, 081802 (2005).
[19] S. Fukuda et al., Nucl. Instrum. Methods A **501**, 418 (2003).
[20] K. Nitta et al., Nucl. Instrum. Methods A **535**, 147 (2004).
[21] K2K MRD Group, T. Ishii, et al., Nucl. Instrum. Methods A **482**, 244 (2002).
[22] A. Suzuki et al., Nucl. Instrum. Methods A **453**, 165 (2000).
[23] B. J. Kim et al., Nucl. Instrum. Methods A **497**, 450 (2003).
[24] C. Walter, Nucl. Phys. B Proc. Supp. **112**, 140 (2002).
[25] R. Brun et al., CERN DD/EE/84-1 (1987).
[26] H. Nakamura and R. Seki, Nucl. Phys. B Proc. Supp. **112** (2002).
[27] H. Nakamura and R. Seki, Nucl. Phys. B Proc. Supp. (2002), proc. NuInt02, Irvine, in press.
[28] S. Boneti et al., Nuovo Cimento A **38**, 260 (1977).
[29] N. Armenise et al., Nucl. Phys. B **152**, 365 (1979).
[30] J. Brunner et al., Z. Phys. C **45**, 551 (1990).
[31] R. Kustom et al., Phys. Rev. Lett. **22**, 1014 (1969).
[32] L. Ahrens et al., Phys. Rev. D **35**, 785 (1987).
[33] L. Ahrens et al., Phys. Lett. B **202**, 284 (1988).
[34] S. Galster et al., Nucl. Phys. B **32**, 221 (1971).
[35] M. G. Olsson, E. T. Osypowski, and E. H. Monsay, Phys. Rev. D **17**, 2938 (1978).
[36] V. Bernard, L. Elouadrhiri, and U.-G. Meissner, J. Phys. G **28**, R1 (2002).